EurJIC
European Journal of Inorganic Chemistry

Research Article
doi.org/10.1002/ejic.202400117

Chemistry Europe
European Chemical Societies Publishing

www.eurjic.org

Supported Ruthenium Phosphide as a Promising Catalyst for Selective Hydrogenation of Sugars

Lukas Popp[+],[a, c] Philipp Kampe[+],[b] Birk Fritsch,[a] Andreas Hutzler,[a] Maximilian J. Poller,[b] Jakob Albert,[b] and Patrick Schühle*[c]

This work demonstrates that supported ruthenium phosphides (RuP_2) are attractive catalysts for selective production of alditols by sugar hydrogenation. In our studies, carbon supported RuP_2 with a ruthenium content of 5 wt.–% led to the highest activity in xylose hydrogenation and to nearly 100% yield for xylitol. ICP-OES and XRD measurements revealed the stability of this novel RuP_2/C catalyst under typical hydrogenation conditions (50 bar_{H2}, 120 °C) in aqueous phase. Furthermore, STEM-EDX illustrated the close proximity of ruthenium and phosphorous on the catalyst site and the formation of nanoparticles in the size of 2–4 nm. The catalyst system was successfully applied for the selective hydrogenation of further sugar substrates, including glucose, fructose, and disaccharides, such as cellobiose and sucrose. Here, the RuP_2/C revealed its bifunctional acidic/metallic character, enabling in a tandem reaction the hydrolysis of disaccharides, directly followed by a selective hydrogenation to form sugar alcohols in high yield.

Introduction

Transition metal phosphides (TMP) have emerged as a compelling class of heterogeneous catalysts, with a particular emphasis on hydrogenation reactions.[1] These materials, which are comprised of transition metals in combination with phosphorus, demonstrate unique catalytic behavior due to their distinctive electronic configurations and surface properties.[2] The development and application of TMPs have shifted into the focus in the field of catalysis, given their potential to bring about transformative changes in hydrogenation processes.[3]

The reason for the usage of TMP catalysts lies in their unique properties. TMPs possess both metal active sites and acid sites, demonstrating activity not only in hydrogenation but also in a number of acid-catalyzed processes.[4] They have physical properties resembling ceramics, making them strong and hard, yet they retain electronic and magnetic properties similar to metals.[5] Furthermore, in contrast to their purely metallic counterparts, TMPs exhibit improved selectivity behavior as well as higher resistances towards common deactivation processes.[6]

In hydrogenation, TMPs have demonstrated the ability to selectively target specific functional groups, while leaving others untouched. This has been shown by Bonita *et al.* during the selective hydrogenation (S = 99%) of benzophenone and benzaldehyde to 1° and 2° alcohols, respectively, using RuMoP. This behavior is attributed to the presence of Lewis acidic sites on the surface that facilitate the hydrogenation of the carbonyl group and prevent hydrodeoxygenation, as well as other undesired side reactions.[7] The tunable selectivity of TMP catalyst renders them particularly beneficial for the hydrogenation of complex biomolecules. Herein, the catalytic hydrogenation of biomass-derived sugars represents a pivotal field within green and sustainable chemistry, driven by the growing demand for renewable and environmentally friendly alternatives to conventional chemical processes.[8] By valorizing sugars from sources such as agricultural residues, food waste, and dedicated energy crops, this transformation contributes to reducing the carbon footprint associated with traditional chemical synthesis.[9]

Xylose is a key precursor for chemicals and biofuels, as well as a vital polyol used in pharmaceutical, food, and cosmetics due to its low calories, tooth-friendly, and diabetic-safe properties. High selectivity and conversion rates are crucial in its synthetic process, especially for pharmaceutical and food sectors where product purity is essential.[10] The hydrogenation step from xylose to xylitol is visualized in Scheme 1. The hydrogenation mechanism of xylose is reported by Wisniak *et al.* and the hydrogenation mechanism of glucose by Brahme *et al.*, both can be described as a first order reaction regarding the sugar as well as the catalyst concentration. Heinen *et al.* recorded a pseudo first order reaction order regarding the hydrogenation of fructose to mannitol.[11]

Sugars are converted to alditols through catalytic hydrogenation, avoiding hydrodeoxygenation or methanolysis. The

[a] L. Popp,[+] Dr. B. Fritsch, Dr.-Ing. A. Hutzler
Forschungszentrum Jülich, Helmholtz Institute Erlangen Nürnberg for Renewable Energy, 91058 Erlangen, Germany

[b] P. Kampe,[+] Dr. M. J. Poller, Prof. Dr.-Ing. J. Albert
Institute of Technical and Macromolecular Chemistry, Universität Hamburg, Bundesstraße 45, 20146 Hamburg, Germany

[c] L. Popp,[+] Dr.-Ing. P. Schühle
Institute of Chemical Reaction Engineering, Friedrich-Alexander-Universität Erlangen-Nürnberg, 91058 Erlangen, Germany
E-mail: Patrick.Schuehle@fau.de

[+] Equal contribution.

Supporting information for this article is available on the WWW under https://doi.org/10.1002/ejic.202400117

Research Article
doi.org/10.1002/ejic.202400117

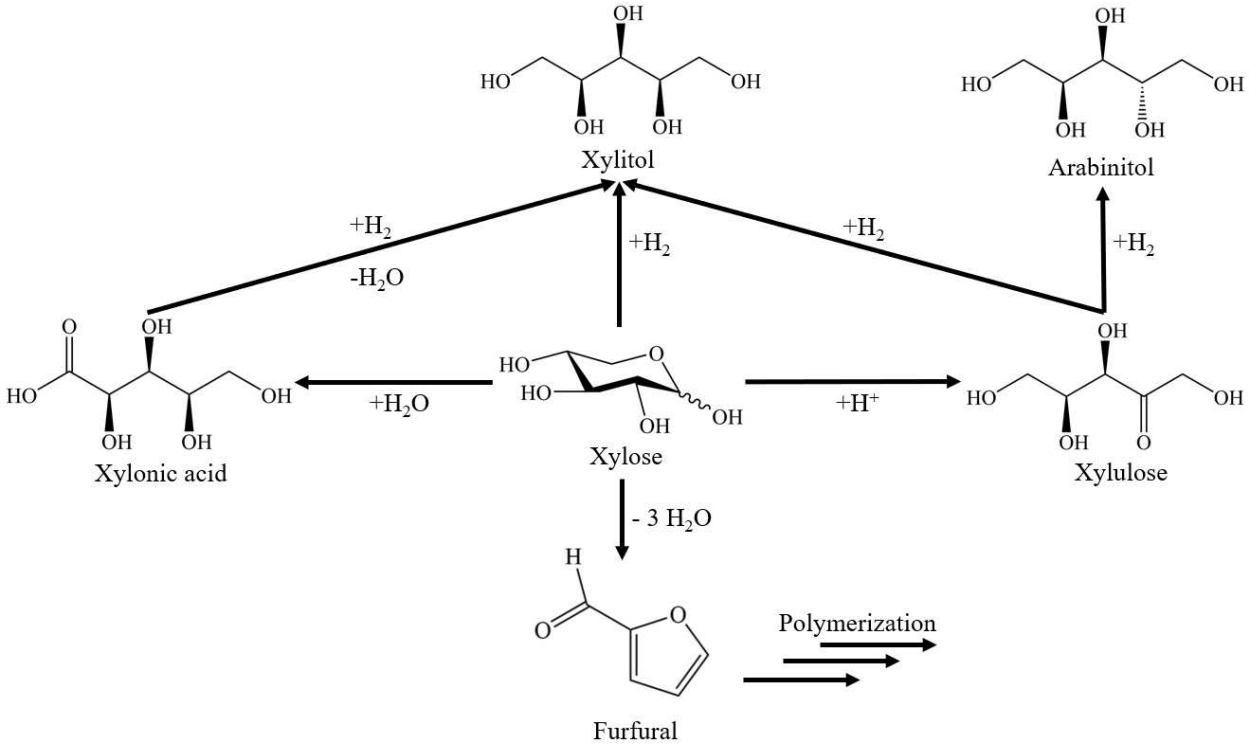

Scheme 1. Hydrogenation of d-xylose to xylitol with possible by products: d-xylonic acid, furfural, d-xylulose, and d-arabinitol.[12]

selectivity toward either xylitol production or methanolysis depends on the initial activation of the carbonyl (C=O) or carbon-carbon (C–C) bond in the sugar reactant. It is reported, that Lewis acidic surface sites initiates a polarization within the organic molecule, thereby amplifying its electrophilicity and consequently its reactivity.[13] The capability of TMP to activate both carbonyl groups as well as hydrogen molecules renders them as excellent catalyst for selective hydrogenation processes.[14–16] Alternatively, base-catalyzed activation of the C–C bond in hydrogenolysis occurs via a retro-aldol mechanism.[17] Thereupon the subsequent generation of methane (CH_4) can be dismissed, as it occurs in parallel rather than as sequential reaction. This is attributed to the activation of either the carbonyl group or the C–C bond. Catalytic systems that consistently differentiate between the activation of a carbonyl and a carbon-carbon moiety are the focus of current research.[18]

Ruthenium containing catalyst show promising selectivity and yield for the conversion of sugars to alditols. It is previously reported that the choice of support material has great benefits to the reaction characteristics. For instance, Al_2O_3 reduces the poisoning mechanisms while HY zeolites display a significant lowering of the activation energy.[19,20] More exotic support materials like hypercrosslinked polystyrene lead to a kinetic control of the synthesis path driven by improved hydrogen spillover.[21] In most cases small amounts of methanolysis are still reported across the board.[20,21]

The implementation of phosphorous either directly to the catalyst or to the reaction mixture has been reported in few studies to have a positive effect on the conversion and selectivity during the hydrogenation of sugars. While the addition to the reaction mixture in form of phosphoric acid showed a positive effect, it was mostly attributed towards the higher H_3O^+ concentration.[22] The first implementation of transition metal phosphides has been reported by Ding *et al.* Herein, the authors reported the conversion of cellulose to sorbitol/mannitol mixtures of 10:1 with a yield of 48.4% using Ni_2P catalyst.[23] Furthermore Yamaguchi *et al.* investigated the activity of hydrotalcite supported Ni_2P nanoparticles (NP) in the hydrogenation of d-xylose to d-xylitol. Herein it is reported, that the influence of the support plays a significant role in the performance of the catalyst, improving the selectivity approximately by factor 100 compared to unsupported Ni_2P-NP.[15,16] In addition to that Qiu *et al.* recently reported a bifunctional Ru_2P/C-SO_3H catalyst for the direct conversion of cellulose to sorbitol at up to 200 °C. Here the bifunctional character is achieved by the acidic surface centers introduced by sulfuric acid. It is stated the ruthenium-based materials reduce the excessive hydrogenation of the formed alditols greatly compared to their phosphorus free counterpart.[24]

Based on the aforementioned results we study a broad selection of supported RuP_2 catalyst for the hydrogenation of monosaccharides, namely d-xylose (C5 sugar), d-glucose (C6 sugar with a carbonyl group), and fructose (C6 sugar with a keto group) as well as the disaccharides sucrose (glucose and fructose connected via a glycosidic bond) and cellobiose (two glucose molecules connected via a glycosidic bond) at lower temperatures compared literature.[24] In the presented research we investigated the influence of the support material on the performance metrics selectivity and conversion. The goal was

Research Article
doi.org/10.1002/ejic.202400117

the selective formation of alditols as well as the investigation of the catalytic performance in a broader spectrum of substrates, compared to previously mentioned studies. The TMP-support interactions were investigated using physi- and chemisorption methods, in addition to composition and structural analysis.

Experimental

Materials

All chemicals were commercially sourced and utilized without additional purification. The materials used for the preparation of the catalyst were anhydrous ruthenium(III)chloride ($RuCl_3$, Merck, 99,9%), anhydrous nickel(II)chloride ($NiCl_2$,Alfa Aesar, >98%), diammonium hydrogen phosphate ($(NH_4)_2HPO_4$, Arcos Organics, >99%), citric acid monohydrate ($C_6H_8O_7$, Merck, >98%), silica support (SiO_2, Sigma Aldrich, 99%), H-β zeolite (SiO_2:Al_2O_3, abcr, >98%), activated carbon (C, Merck, >98%), nitrogen (N_2, Air Liquide, 99,99%), hydrogen (H_2 Air Liquide, 99,99%) and argon (Ar, Air Liquide, 99,99%). For the hydrogenation experiments d(+)-xylose ($C_5H_{10}O_5$, Merck, >98%), d(+)-glucose ($C_6H_{12}O_6$, Merck, >98%), d(−)-fructose (Merck, $C_6H_{12}O_6$, >99%), sucrose ($C_{12}H_{22}O_{11}$, Alfa Aesar, 99%), d(+)-cellobiose ($C_{12}H_{22}O_{11}$, Carl Roth, >98%) and millipore water were used.

Catalyst Preparation

The synthesis of the different TMP materials was adapted from a previously reported temperature programmed reduction (TPR) procedure.[25] Aqueous solutions containing the metal precursor ($RuCl_3$ or $NiCl_2$), $(NH_4)_2HPO_4$, and citric acid (0.7 mol per mol of metal) were prepared. Citric acid was added to increase the surface area of the resulting catalyst and to reduce the formation of large particles. The molar ratio of the metal and phosphorous precursor was adjusted to 1:4 to guarantee a full conversion of the metal precursor. This ratio has previously been determined in validation experiments in the reaction set up. The supported catalysts were synthesized by incipient wetness impregnation by mixing the support materials and the prepared solutions, followed by drying at 90 °C for 24 h. The material was calcined at 550 °C for 6 h under 5 $NL_{Ar}\,min^{-1}$ with a heating ramp of 2 $K\,min^{-1}$ in a muffle furnace. Following a previously reported procedure, the calcined catalyst was subsequently reduced in a tube furnace at 750 °C for Ni-based and at 850 °C for Ru-based material for 6 h using a 10 $K\,min^{-1}$ heating ramp.[6] These high temperatures have been chosen to synthesize a single phase TMP, as it is reported in literature.[26] The materials were reduced under N_2-diluted H_2 flow (18 $ml_{H2}\,min^{-1}$, 142 $ml_{N2}\,min^{-1}$). The reduced materials were passivated under synthetic air flow (160 $ml_{syn.air}\,min^{-1}$) for 1 h.

Catalyst Characterization

The success of the metal phosphide phase formation was evaluated by both, the solid-state structure, as well as the metal/phosphorous ratio (M/P ratio) of the product.

The solid-state structure of the prepared materials was determined using powder X-ray diffraction (XRD). The measurements were carried out in angles of 10–90 °2θ, a scanning speed of 0.02°/s, a step size of 0.015° and 100 s time per step on a X'Pert Pro by Malven Panalytics. Cu–Kα was used as the radiation source and X'Celerator as the detector. The data was processed utilizing X'Pert Highscore Plus and compared to simulated reflexes from the inorganic crystal structure database (ICSD).

Material composition before and after the hydrogenation reactions were measured via inductively coupled plasma-optical emission spectroscopy (ICP-OES). Approximately 100 mg of samples supported on either SiO_2 or H-β zeolite were dissolved using microwave-assisted digestion at 220 °C in a solution containing HCl, HNO_3 and HF (6:2:2 ml). The solutions were measured in an ICP-OES Ciros CCD from Spectro Analytical Instruments GmbH. Desired elements such as Ni, Ru, and P were calibrated using standard solutions. Three consecutive measurements of the dissolved samples were carried out and an average value was calculated.

The samples containing ruthenium and carbon were handled differently. A method reported by Suronate *et al.* for ruthenium and carbon containing catalysts was adapted for the determination of the ruthenium and phosphorous content of the samples.[27] Approximately 100 mg of a sample was placed in a ceramic vessel within a preheated muffle furnace (200 °C) and further heated to 450 °C with a rate of 5 $K\,min^{-1}$ and held for 2 h. After cooling down, 380 mg KOH and 650 mg KNO_3 were added to the crucible, mixed with the sample, and heated up again to 450 °C with a heating ramp of 5 $K\,min^{-1}$. The temperature was held for 1 h. To stabilize the Ru and mainly RuO_4^{2-}, 50 mg $K_2S_2O_8$ was added to the cold sample and the melts were dissolved in approx. 5 ml millipore water. 10 ml of 1 M KOH were introduced, and the solution was transferred to 100 ml volumetric flasks and further diluted. The elemental composition was measured by ICP-OES as described above.

The sulfur content of the purchased support materials was analyzed via carbon, hydrogen, nitrogene, sulfur (CHNS) elemental analysis using a Unicube by Elementar Analysensysteme GmbH. The samples were reduced at 850 °C followed by a combustion at 1050 °C. These measurements were conducted to investigate catalyst purity after synthesis.

The surface area, as well as the pore volume of the synthesized material was determined by N_2-Sorption on a Quantachrome Quadrasorb SI-MP-8. The samples were degassed at approximately 2 10^{-5} bar for 12 h at 250 °C. The relevant values were determined applying the Brunauer-Emmett-Teller (BET) theory.

Temperature programmed desorption of ammonia (NH_3-TPD) was conducted on the same measuring device. In the initial stage, the material was loaded with ammonia. To achieve this, the material was initially heated to 200 °C to remove surface bound water, followed by its exposure to a helium gas stream containing 10% ammonia at a temperature of 200 °C for a duration of one hour. In the following desorption step the loaded material was heated up to 700 °C at 10 °C min^{-1} in a helium gas flow at 20 $cm^3\,min^{-1}$. The temperature was maintained at its final value for a duration of one hour.

The nanostructure of the catalyst particles wads analyzed via high-angle annular dark field scanning transmission electron microscopy (HAADF-STEM). To do so, a Thermo Fisher Scientific Talos F200i (S)TEM microscope was employed at 200 kV acceleration voltage. Elemental mapping by energy-dispersive x-ray spectroscopy (STEM-EDX) was performed using a Dual Bruker XFlash 6|100 EDX detector. Image analysis was facilitated using FIJI by measuring the projected area of particles in HAADF-STEM.[28]

Catalyst Testing

The reduction of sugars to their corresponding alcohols via hydrogenation was performed simultaneously in a 10-fold reaction

Research Article
doi.org/10.1002/ejic.202400117

Table 1. Hydrogenation of xylose using RuP_2 and Ni_2P on SiO_2, reaction conditions: T = 120 °C, $p_{Hydrogen}$ = 50 bar, t = 20 h, stirrer speed = 500 min^{-1}. The control experiment was performed without catalyst or support, using identical reaction conditions.

	Metal loading/wt%	X_{Xylose}/%	$S_{Xylitol}$/%
Ni_2P on SiO_2	5.74	14.3	33.1
RuP_2 on SiO_2	5.10	81.1	99.8

system using 21 mL high-pressure stainless-steel (1.4571) vessels. For each experiment, 100 mg of the catalyst was added to a 10 mL aqueous substrate solution (0.55 mol*L^{-1}) with a polytetrafluorethylen (PTFE)-coated stirrer bar. The reactors were then closed, placed above a magnetic stirrer in a heating block and connected to the gas supply.

First, the reactors were purged three times with N_2 in order to remove residual air. Then the reactors were pressure tested at 50 bar N_2, before they were purged again three times with H_2 (5.0 grade, Linde) and finally filled with approx. 40 bar of H_2 at room temperature. Then the reactors were heated to 120 °C under stirring with 300 rpm to reach a reaction pressure of approx. 50 bar. Then the stirrer speed was increased to 500 rpm. This point was defined as starting time for the reaction. After 20 h the reactors were taken out of the heating block and cooled down to room temperature.

Analysis of the Reaction Products

The gas phase was taken from the reactors using a gas bag and analyzed by a Varian GC 450 equipped with a Shin-carbon ST column (2 m ×0.75 mm) and both, a thermal conductivity conductor (TCD) and a flame ionization detector (FID) detector. Argon was used as the mobile phase.

The catalyst was filtered off, washed with millipore water, and dried for further analysis.

Products in the liquid phase were identified by Nuclear magnetic resonance spectroscopy (NMR) and quantified using a high-performance liquid chromatography (HPLC) system from SHIMADZU equipped with an Aminex HPX-87 H 300 mm ×7.8 mm BIORAD Column and a refractive index detector. An aqueous sulfuric acid solution (5 mmol*L^{-1}) was used as eluent.

^{13}C nuclear resonance spectroscopy (^{13}C-NMR) was measured using a Bruker Avance III HD 400 MHz. The samples were prepared by adding 0.7 mL reaction solution to 0.07 mL D_2O. Calculation details are given in the SI.

ICP-OES was used to determine leaching of elements from the catalysts in the reaction solution. Characterization was done on an ASCOR-spectrometer (Fa. Spectro). Phosphate was quantified using ion chromatography (IC) on an ICS-1100 (Fa. Dionex/Thermo).

Results and Discussion

The heterogeneously catalyzed hydrogenation of sugars is mostly carried out under the use of either noble metal catalyst (i.e., Ru, Pd, Pt) or Raney-Nickel, whereas Ru shows the highest conversion and selectivity compared to Ni, Pd and Pt in the order given.[29] Following this, nickel- (5.7 wt% on SiO_2) and ruthenium-based (5.1 wt% on SiO_2) phosphide catalysts were synthesized and tested in the hydrogenation of xylose (see Table 1).

RuP_2 showed better performance (X = 81.1 %, $S_{Xylitol}$ = 99.8 %) compared to the Ni_2P catalyst (X = 14.3 %, $S_{Xylitol}$ = 33.1 %). In addition, RuP_2 demonstrated a significantly higher stability against leaching of the active phase from the support material and destruction of the crystalline phosphide phase as seen from the XRD-results (see Figure 1) and the metal loading (see Table 2) before and after reaction. While RuP_2 on SiO_2 shows no additional reflexes after the hydrogenation of xylose, Ni_2P on

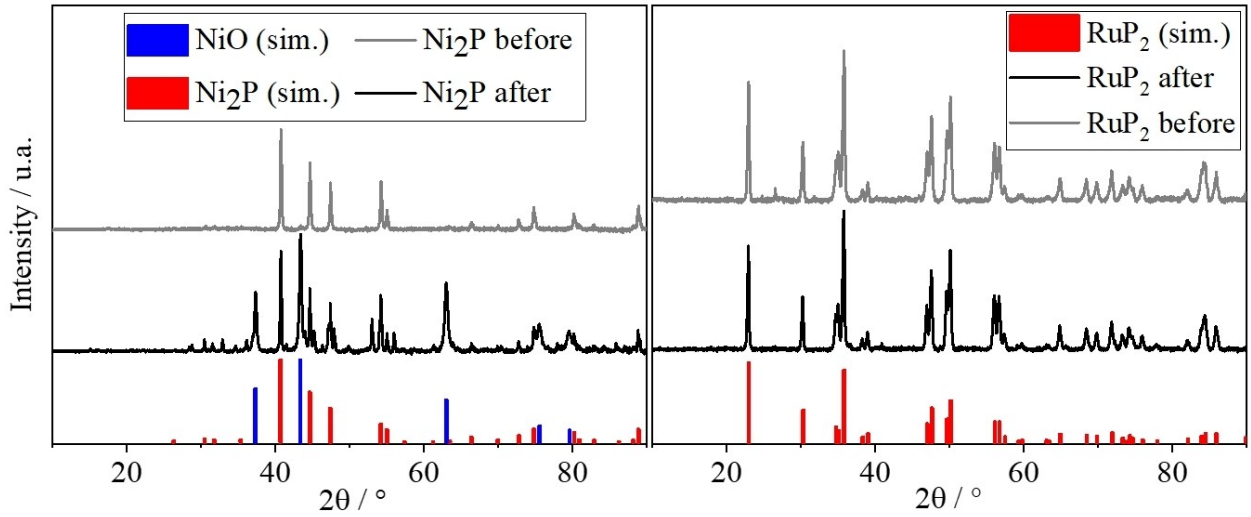

Figure 1. XRD patterns of the catalyst Ni_2P on SiO_2 (left) compared to the simulated reflexes of Ni_2P (ICSD-reference code: 98–064-6102) and NiO (ICSD-reference code: 98–000-9866), as well as RuP_2 on SiO_2 (right) compared to the simulated reflexes of RuP_2 (ICSD-reference code: 98–000-0992), before (grey) and after (black) the hydrogenation of xylose.

Research Article
doi.org/10.1002/ejic.202400117

Table 2. Metal loading (wt%) and metal/phosphorous ratio determined by ICP-OES before and after the hydrogenation of xylose.

	Before		After	
	Loading/ wt%	M/P ratio/–	Loading/ wt%	M/P ratio/–
Ni_2P on SiO_2	5.74	2.04	3.82	5.52
RuP_2 on SiO_2	5.10	0.45	5.00	0.47
RuP_2 on activated carbon	4.48	0.33	4.51	0.41
RuP_2 on H-β zeolite	4.97	0.42	5.00	0.49

SiO_2 indicates the formation of a crystalline NiO phase (reflexes appear at 37°, 43°, 63°, 76° and 80°). This can be attributed to the disintegration of the active Ni_2P phase and subsequent oxidization of the Ni phase. This assertion is further substantiated by the ICP-OES results obtained from the catalyst post reaction. M/P ratios of 2.0 for NiP_2 and 0.5 for RuP_2 are expected from the stoichiometry of the TMPs, which are well achieved for both catalysts after synthesis. While metal loading and M/P ratio of the RuP_2 on SiO_2 stays constant after reaction, significant decrease of nickel loading, and phosphorous content were observed for the Ni_2P-based sample. This change indicates the removal of bound phosphorous and thus a disintegration of the active phase. Please note, that such phosphorus leaching from Ni_2P in aqueous phase sugar conversion was also observed by Ding et al.[23] Overall, RuP_2 revealed higher activity and stability in the hydrogenation of xylose and was therefore selected for further studies.

Variation of the Catalyst Support

A series of experiments was conducted to determine the influence of the support material for the selected RuP_2 structure on both, the catalytic performance, and the catalyst stability. Therefore, RuP_2 was supported on SiO_2, activated carbon (C) and H-β-zeolite and compared in the hydrogenation of xylose. The conversion and selectivity of these hydrogenation experiments are shown in Figure 2. The supported RuP_2 catalysts are compared to both bulk RuP_2 and a control experiment without catalyst. The benchmark experiment with the neat support materials only showed small conversions below 9% (see Figure S1 in SI).

Among the supported catalysts, RuP_2/C showed complete conversion with a selectivity of 99.9% regarding xylitol production after a reaction time of 20 h. The catalyst on the other support materials reached comparable selectivity towards the formation of xylitol (H-β zeolite: 81.6%; SiO_2: 99.8%). While the conversion for RuP_2 on H-β zeolite was significantly lower (H-β zeolite: 11.8%) RuP_2 on SiO_2 showed marginally lower conversion (SiO_2: 81.1%). The blank experiment without catalyst resulted in a conversion of only 1.2%. The bulk RuP_2 showed a conversion of 47.0% and a selectivity towards xylitol of 93.4%. Other products were identified as levulinic acid (S = 4.0%) and methane (S = 0.7%). Ru/C on the other hand, while displaying high conversion (X > 99,9%), shows a lower selectivity towards alditol formation compared to the tested TMP catalyst, with a rather high selectivity towards methanolysis (S = 31,2%). As a consequence, the special relationship between phosphorus and the ruthenium metal and presumably also electronic effects introduced by phosphorus in the surrounding of the ruthenium metal are crucial for the selectivity This leads to the conclusion

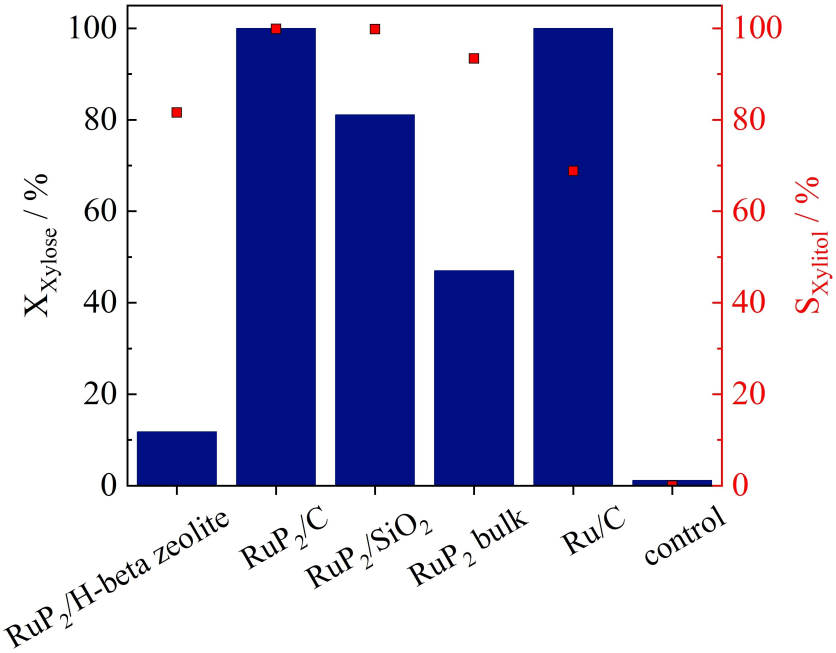

Figure 2. Hydrogenation of xylose using RuP_2 on varying support (5 wt% regarding Ru), as bulk material, and Ru/C (5 wt% Ru) reaction conditions: T = 120 °C, $p_{Hydrogen}$ = 50 bar, t = 20 h, stirrer speed = 500 min^{-1}. The control experiment was performed without catalyst or support at identical reaction conditions.

Research Article
doi.org/10.1002/ejic.202400117

that, while RuP_2 is a highly active catalyst for the hydrogenation of xylose, choosing carbon as a support facilitates the formation of alditols and results in a highly selective catalyst for the hydrogenation of xylose in aqueous solution.

Stability of the different supported RuP_2-catalysts was evaluated by comparing metal loading and M/P ratio of the materials before and after reaction (see Table 2). For the activated carbon and H-β zeolite supported materials, the ruthenium loading stayed fairly constant on a value around 5 wt% during reaction. The M/P ratio was below the expected stoichiometric value of 0.5 for these catalysts after synthesis, indicating the presence of phosphorous, that is not bound in the crystal structure. The M/P ratios for the RuP_2 catalysts shifts closer to the optimal 0.5, suggesting the removal of unbound phosphorous during the reaction.

To further study potential phosphorous and ruthenium leaching, the product solutions of the hydrogenation reactions were analyzed regarding its phosphorous (ICP-OES) and phosphate (IC) content (see Table 3). A phosphorous/phosphate (P/PO_4^{3-}) ratio of 0.340 would indicate, that the total leached phosphorous is present in the form of PO_4^{3-} ions in the product solution.

Table 3. Ruthenium and phosphorous leaching in the liquid product phase measured by ICP-OES and IC.

	Ruthenium/ mg L^{-1}	Phosphorous (P)/mg L^{-1}	Phosphate (PO_4^{3-})/ mg L^{-1}	P/ PO_4^{3-} ratio
RuP_2 on SiO_2	< 1	20.0	65.60	0.319
RuP_2 on activated carbon	< 1	73.4	219.0	0.335
RuP_2 on H-β zeolite	< 1	54.3	173.0	0.441

As Table 3 shows, leaching of ruthenium into the product solution was not detected. In contrast, phosphorous leaching into the product phase was observed for all catalyst samples. The amount of phosphorous found in the liquid product phase by ICP-OES and IC analysis coincides with the losses recorded by the ICP-OES analysis of the washed catalyst material (see Table 2). Comparison of ICP-OES and IC of the liquid reaction product display a P/PO_4^{3-}-ratio that is close to the above introduced theoretical value of 0.340. This suggests that phosphorous leaches in form of PO_4^{3-}species that have their origin in non-converted phosphorous precursor on the catalyst, rather than the decomposition of the RuP_2 phase. This is further indicated by the absence of other crystalline phases than RuP_2 in the XRD analysis (see SI, Figure S2) and the M/P ratio, which comes closer to the optimal 0.5 after the catalytic application of the catalysts.

To shed light on the reason for the difference in hydrogenation activity, the surface acidity of the different supported RuP_2-catalysts was investigated by NH_3-TPD. The results of the NH_3-TPD are illustrated in Figure 3. The NH_3-TPD spectra can be divided in three distinct peaks, which exhibit varying degrees of overlap. The low temperature peaks (T < 400 °C) can be attributed to weak acidic centers. The high temperature peak, in turn, is ascribed to strong acidic centers.[30] The results show that strong binding surface centers with a desorption temperature above 400 °C are not detected for RuP_2 supported on SiO_2 and H-β zeolite, while the carbon supported sample shows a clear high temperature signal. These strong acidic sites are a possible reason for the higher conversion of RuP_2/C, due to favored adsorption and activation of the carbonyl group and thus a faster hydrogenation of xylose. Brønsted acidity would lead to the formation of hydroxymethylfurfural (HMF), while

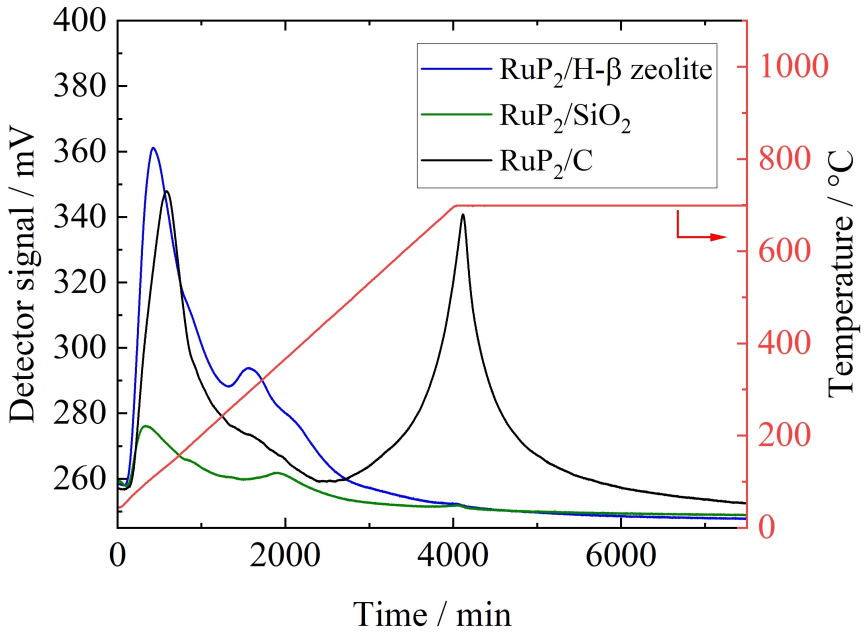

Figure 3. NH_3-TPD results of RuP_2 (5 wt%) supported on H-β zeolite (blue), SiO_2 (green) and activated carbon (C, black).

Research Article
doi.org/10.1002/ejic.202400117

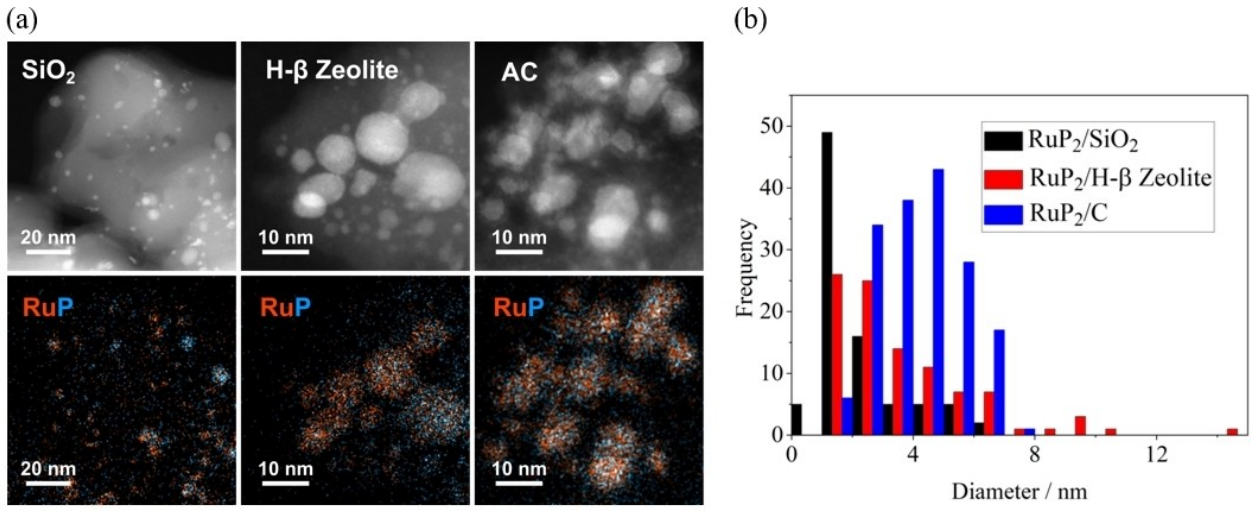

Figure 4. (a) Structural and compositional analysis of the investigated catalyst using HAADF-STEM and EDX spectrum imaging (5 wt% RuP_2 on SiO_2/left, H-β zeolite/middle and activated carbon/right); blue: phosphorous, red: ruthenium. (b) particle size distribution of 5 wt% RuP_2 on SiO_2/black, H-β zeolite/red and activated carbon/blue.

Lewis acidity catalyzes the formation of alditols. As no formation of either HMF or subsequent polymerization products could be detected, it is assumed, that these acidic centers are indeed Lewis acidic.[31] An exact determination of Lewis/Brønsted acidity would require isotope-ratio mass spectrometry (IRMS)-NH_3-TPD, which was not available at the time of data acquisition.[32] While no NH3-TPD for RuP_2/C is reported in Literature, no strong acidic centers can be reported for other supports or other Ru containing TMPs.[33]

To investigate the morphology of the supports and catalysts, N_2-physisorption was performed, characterizing the available surface area and pore volume before and after the synthesis. For comparison, the support material underwent only thermal treatment under conditions similar to the synthesis parameters of RuP_2 (850 °C, 18 ml $_{H2}$ min^{-1}, 142 ml_{N2} min^{-1}, 6 h) in a further test series. The N_2-physisorption results are listed in Table 4.

In the synthesis of RuP_2, activated carbon retains approximately 75% of its initial surface area and 91% of its initial pore volume. In contrast, both SiO_2 and H-β zeolite experience significant reductions in their initial surface areas and pore volumes, retaining only 15% and 14% of their initial surface areas, and 15% and 23% of their initial pore volumes, respectively. Based on this data, it is assumed that the significantly higher surface area/pore volume and consequently higher number of active sites are one of the main reasons for the higher activity during the hydrogenation of xylose. This tremendous surface reduction is only observed when the combination of the incipient wetness impregnation method and the high synthesis temperatures are applied. After thermal treatment of the pure supports, in contrast, only a slight decrease of surface area and pore volume was observed.

To further characterize the surface of the catalyst, HAADF STEM-EDX measurements were conducted. The Maps (a) as well as the particle size distribution (PSD)(b) are displayed in Figure 4.

The EDX maps show that phosphorus and ruthenium can be found at the same locations. No excessive spot-formation of either element can be observed. This suggests a homogeneous distribution of both elements within the nanoparticles. RuP_2 on SiO_2 display a rather narrow PSD, while the other support materials show a broader distribution. It is assumed, that two particle formation processes take place. Firstly, the formation of primary particles (2–6 nm) followed by the agglomeration of secondary particles (> 8 nm). These two regimes are especially pronounced for RuP_2 on H-β zeolite. In addition to the spectrum images the ruthenium particle size distribution, mean particle diameter of the equivalent projection area and the ruthenium dispersion (see Table 5) were calculated on the basis of the STEM-Images and the specific surface of one ruthenium atom.[34]

Table 4. BET surface area and pore volume of the untreated and temperature treated support materials, as well as of the supported RuP_2 (5 wt%) catalyst, measured via N_2-physisorption.

	BET surface area/$m^2 g^{-1}$			Pore volume/$ml g^{-1}$		
	Carbon	SiO_2	H-β zeolite	Carbon	SiO_2	H-β zeolite
Untreated support	868	483	605	0.70	0.78	0.39
RuP_2 on support	650	72	84	0.64	0.12	0.09
Temperature treated support (850 °C)	675	472	606	0.66	0.80	0.40

Research Article
doi.org/10.1002/ejic.202400117

Table 5. Calculated ruthenium dispersion and mean particle diameter of 5 wt% RuP_2 on different supports.

Support	C	SiO_2	H-β zeolite
Ru-Dispersion/%	26.1	31.5	18.2
Mean particle diameter / nm	4.1 ± 1.3	2.3 ± 1.4	3.6 ± 2.4

The RuP_2 catalyst, when supported on H-β zeolite, exhibits the lowest dispersion of only around 18.2%. In contrast, silica, and activated carbon, despite having comparable dispersion levels of 31.5% and 26.1%, demonstrate a discrepancy in their performance in the hydrogenation of xylose. This discrepancy can presumably be attributed to the pronounced influence of the acidic surface centers inherent to the activated carbon, which contribute to its higher conversion rate. Alternatively, it is suggested that pores are blocked due to the impregnation technique as well as the high synthesis temperature, indicated by the low surface area and low pore volume. It is assumed that these pores are clogged by the formation of larger particles and agglomerates caused by the high temperature during the material synthesis, denying access to active metal centers. As activated carbon showed much higher resistance against this effect the following experiments, activated carbon was chosen as the support for RuP_2, due to its superior catalytic performance.

Variation of the Metal Loading

For the subsequent set of experiments, RuP_2 materials with ruthenium loadings of 1, 2.5, and 10 wt% were used in addition to the previously used 5 wt% RuP_2 on activated carbon to investigate the influence of the metal loading on the catalytic performance in xylose hydrogenation. The conversion and selectivity, reached in these experiments are displayed in Figure 5.

During the experiment, catalysts with 1 wt% and 2.5 wt% RuP_2 on activated carbon achieved conversions of 58.2% and 91.3%, respectively. However, the catalysts with 5 wt% and 10 wt% RuP_2 both reached complete conversion after a reaction time of 20 hours. Furthermore, no by-products were detected during the process, and a xylitol selectivity of >99.9% was recorded, even at full xylose conversion.

Regarding the stability of the differently loaded catalysts, no ruthenium leaching could be detected. The phosphorous leaching, calculated from the ICP-OES of the catalyst before and the reaction, as well as the results obtained from ICP and IC of the liquid samples correspond to the previous experiments (see Table 3) and are displayed in the SI (Table S1 and Table S2). In addition, XRD analysis of these samples after reaction shows no change in the crystal structure (see SI, Figure S4).

Substrate Variation

The following series of experiments were designed to evaluate the applicability of the 5 wt% RuP_2 on activated carbon catalyst across different sugar substrates. In addition to d-xylose (C5-

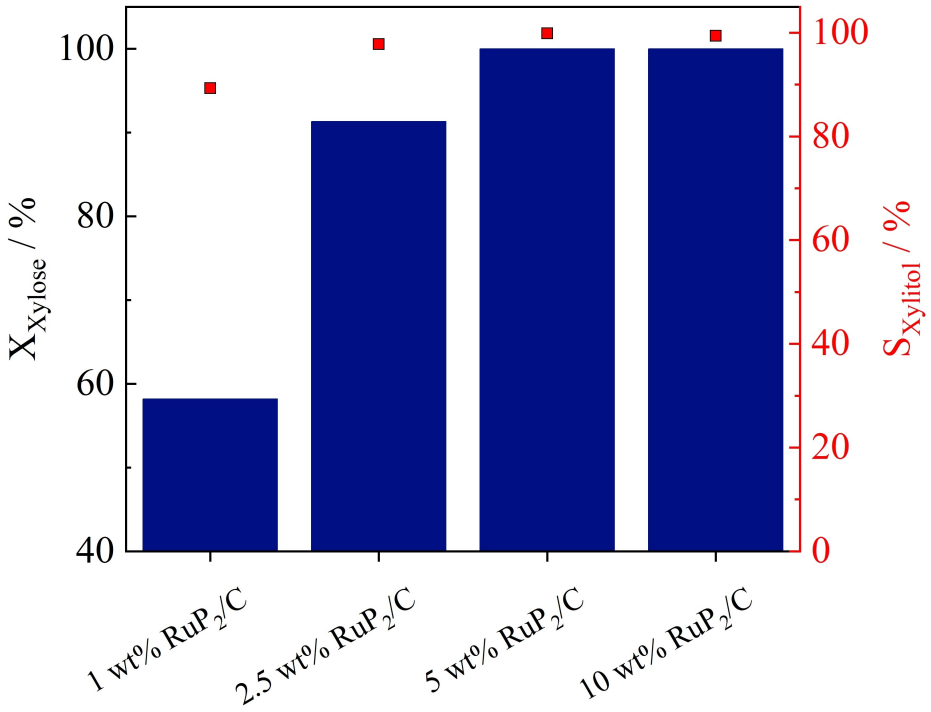

Figure 5. Hydrogenation of xylose using RuP_2 on activated carbon with varying metal loading (1, 2.5, 5, 10 wt%), reaction conditions: T = 120 °C, $p_{Hydrogen}$ = 50 bar, t = 20 h, stirrer speed = 500 min^{-1}).

Research Article
doi.org/10.1002/ejic.202400117

sugar), d-glucose (C6-sugar with a carbonyl group), fructose (C6-sugar with a keto group) and the disaccharides sucrose (d-glucose and fructose linked) and cellobiose (two d-glucose molecules linked) were deployed as substrates in the hydrogenation experiments. The results of these experiments are presented in Figure 6. It can be observed that for all the investigated substrates, apart from cellobiose ($X_{Cellobiose} = 50\,\%$), full conversion was achieved after 20 h reaction time. More details of the substrates before and after hydrogenation with their corresponding products are displayed in the ^{13}C-NMR spectra in the SI (Figure S6–S10). Except for the reaction using glucose as substrate, other products than the respective alditol could not be detected. Even with glucose, sorbitol was clearly the main product with a selectivity of 96.2 %. Regarding fructose, a racemic product mixture was identified containing sorbitol and mannitol ($S_{Sorbitol} = S_{Mannitol} = 50.0\,\%$). The racemic mixture is formed due to the non-stereoselective hydrogenation of the keto group (see SI, Figure S11 and Figure S12). The same effect leads so a 3 : 1 sorbitol:mannitol ratio in the hydrogenation of sucrose (see Figure S13). Sucrose consists of a glucose and a fructose molecule that are α,β-1,2-glycosidic connected. In a first step, the glycosidic bond is cleaved, and the resulting glucose and fructose are hydrogenated resulting in the detected statistical product distribution. Regarding the selectivity of the hydrogenation of sucrose, similar ratios have been reported in literature.[35] The direct hydrogenation and hydrolysis of cellobiose has been reported to be a challenging reaction, that usually requires the addition of acids to the solution or the usage of specially prepared support materials.[36,37] In this study, a higher selectivity ($S_{Sorbitol} = 99.3\,\%$) towards sorbitol formation can be reported compared to the literature ($S_{Sorbitol,\ Max} = 84.0\,\%$), without the further usage of additives.[36] It is assumed, that the role of the aforementioned additives is taken by the acidic surface sites of the RuP_2 on activated carbon catalyst, that have been investigated previously (see Figure 3). The final conversion was 48.9 % and is comparable with the average conversion rate reported in literature.[36,37] This demonstrates that RuP_2 on activated carbon is a suitable catalytic system for the highly selective hydrogenation of varying sugar substrates to the respective alditols.

Finally, a series of recycling experiments was performed using the 10 wt % RuP_2/C catalyst in the hydrogenation of glucose. Therefore, the catalyst was cleaned using millipore water, weighed and the sugar content adjusted to the new catalyst mass. Full conversion over four consecutive runs and only a slight decrease in xylitol selectivity was detected (See SI, Figure S5), what might occur due to increased C–C instead of C=O bond activation. However, in the analysis of the recycled catalyst no Ru leaching could be observed (see SI, Table S3). Also, the phosphide structure remained stable as shown by ICP and XRD measurements after catalytic application (see SI, Figure S14 and Table S4).

Conclusions

Transition metal phosphides are a class of heterogeneous catalysts, that promise high performance in selective hydrogenation reactions. In this study, RuP_2/C has been shown to be a superior catalyst for the hydrogenation of sugars to their respective alcohols. RuP_2 was identified as a stable catalyst with high activity and selectivity in xylose hydrogenation, while a

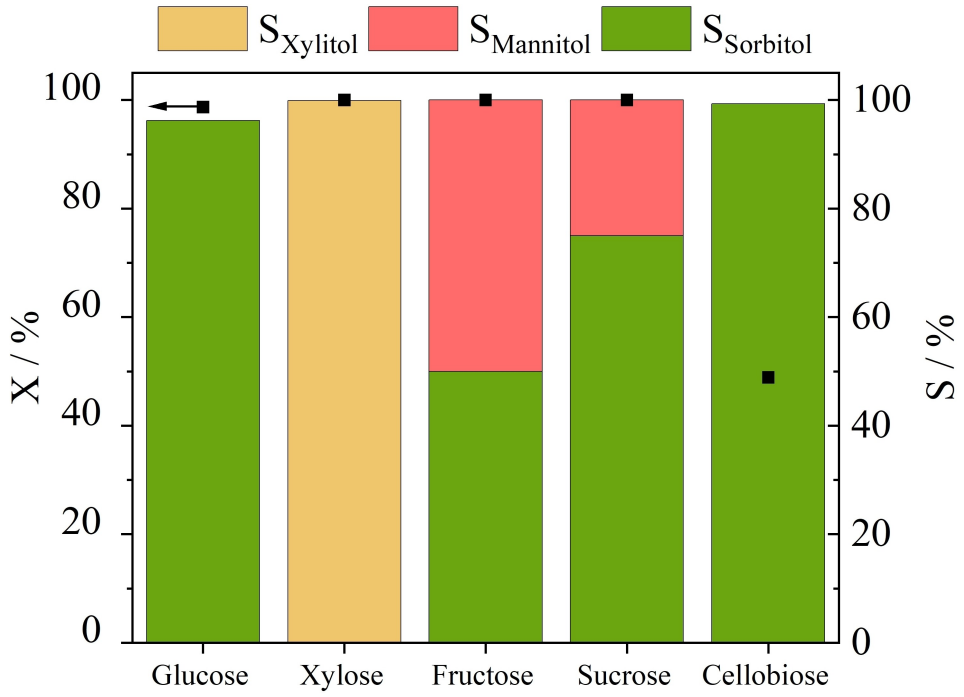

Figure 6. Hydrogenation of different sugars using 5 wt % RuP_2 on activated carbon, Reaction conditions: T = 120 °C, $p_{Hydrogen}$ = 50 bar, t = 20 h, stirrer speed = 500 min^{-1}).

Research Article
doi.org/10.1002/ejic.202400117

previously reported nickel phosphide catalyst (Ni_2P) proved to be less active, and suffered from severe metal leaching and phase transformation. The study further examined the influence of different support materials, namely silica, activated carbon, and H-β zeolite. Activated carbon was identified as the optimal support for the RuP_2 particles among the tested alternatives, attributed to its strong acidic sites, which seem to enhance the activation of the xylose carbonyl group. Furthermore, the alternative supports suffered from severe reduction of available surface area after the impregnation with the ruthenium phosphide. The versatility of RuP_2/C for selective sugar hydrogenation was assessed by investigating its performance for diverse sugar substrates, involving C5- and C6 sugars, as well as disaccharides. Full selectivity to the respective sugar alcohols was observed with all these substrates ($S > 96.2\,\%$) while side product formation by C–C bond breaking was fully suppressed. Due to the acidic properties of the RuP_2/C catalyst, even the disaccharides were converted to the monoalditols in high amount ($X_{Sucrose} > 99\,\%$, $X_{Cellobiose} = 50\,\%$), a distinct advantage of the new bifunctional catalytic system. Moreover, recycling of the 10 wt% RuP_2/C catalyst showed stable activity over five consecutive runs without any detectable Ru leaching. The phosphide structure remained also stable as shown by ICP and XRD measurements post catalysis. However, the slight decrease in xylitol selectivity might be due to improved C–C instead of C=O bond activation.

Authorship contribution statement

LP: Data curation, formal analysis, investigation, methodology, visualization, writing – original draft. PK: Data curation, formal analysis, investigation, methodology, visualization, writing – review and editing. AH, BF: Data curation, formal analysis, visualization, writing – review and editing. MP: Supervision, writing – review and editing. PS, JA: Conceptualization, Project administration, Supervision, writing – review and editing.

Acknowledgements

The author LP acknowledge the technical and finance support of the state of Bavaria and the author PK thanks the Hanseatic City of Hamburg as well as the Central Analytics Department for IC and ICP-OES measurements and the NMR Spectroscopy Facility are acknowledged for NMR measurements at Hamburg University. Open Access funding enabled and organized by Projekt DEAL.

Conflict of Interests

The authors declare no conflict of interest.

Keywords: Transition metal phosphides · ruthenium phosphide · sugar hydrogenation · selective hydrogenation · sugar alcohols

[1] a) L. I. Al-Ali, O. Elmutasim, K. Al Ali, N. Singh, K. Polychronopoulou, *Nanomaterials (Basel, Switzerland)* **2022**, *12*(9), 1435; b) P. Chandra, S. Chakroborty, K. Pal, *Top. Catal.* **2022**, *65*, 1821–1859.
[2] R. Prins, M. E. Bussell, *Catal. Lett.* **2012**, *142*, 1413–1436.
[3] M. J. Ndolomingo, N. Bingwa, R. Meijboom, *J. Mater. Sci.* **2020**, *55*, 6195–6241.
[4] M. A. Golubeva, E. M. Zakharyan, A. L. Maximov, *Pet. Chem.* **2020**, *60*, 1109–1128.
[5] S. T. Oyama, T. Gott, H. Zhao, Y.-K. Lee, *Catal. Today* **2009**, *143*, 94–107.
[6] R. Stöber, F. Mai, O. Sebastian, A. Körner, A. Hutzler, P. Schühle, *ChemCatChem* **2022**, *14*, e202200371.
[7] Y. Bonita, T. P. O'Connell, H. E. Miller, J. C. Hicks, *Ind. Eng. Chem. Res.* **2019**, *58*, 3650–3658.
[8] a) M. Sherbi, J. Albert, *Comput. Chem. Eng.* **2021**, *155*, 107546; b) M. Sherbi, M. Stuckart, J. Albert, *Biofuels Bioprod. Biorefin.* **2021**, *15*, 1431–1446.
[9] M. J. B. Kabeyi, O. A. Olanrewaju, *Front. Energy Res.* **2022**, *9*, 743114.
[10] a) A. Ochoa-Chacón, A. Martinez, H. M. Poggi-Varaldo, L. Villa-Tanaca, A. C. Ramos-Valdivia, T. Ponce-Noyola, *BioEnergy Res.* **2022**, *15*, 905–923; b) Z. Zhao, M. Xian, M. Liu, G. Zhao, *Biotechnology for biofuels* **2020**, *13*, 21; c) A. Gasmi Benahmed, A. Gasmi, M. Arshad, M. Shanaida, R. Lysiuk, M. Peana, I. Pshyk-Titko, S. Adamiv, Y. Shanaida, G. Bjørklund, *Appl. Microbiol. Biotechnol.* **2020**, *104*, 7225–7237; d) V. Jain, S. Ghosh, *Biomass Conv. Bioref.* **2023**, *13*, 9643–9661.
[11] a) A. W. Heinen, J. A. Peters, H. van Bekkum, *Carbohydr. Res.* **2000**, *328*, 449–457; b) J. Wisniak, M. Hershkowitz, R. Leibowitz, S. Stein, *Product R&D* **1974**, *13*, 75–79; c) P. H. Brahme, M. U. Pal, G. Narsaimhan, *Brit. Chem. Eng.* **1964**, *9*, 685–699.
[12] J.-P. Mikkola, R. Sjöholm, T. Salmi, P. Mäki-Arvela, *Catal. Today* **1999**, *48*, 73–81.
[13] a) Y. Román-Leshkov, M. E. Davis, *ACS Catal.* **2011**, *1*, 1566–1580; b) M. Vannice, *J. Mol. Catal.* **1990**, *59*, 165–177.
[14] S. Fujita, S. Yamaguchi, J. Yamasaki, K. Nakajima, S. Yamazoe, T. Mizugaki, T. Mitsudome, *Chemistry (Weinheim an der Bergstrasse, Germany)* **2021**, *27*, 4439–4446.
[15] S. Yamaguchi, S. Fujita, K. Nakajima, S. Yamazoe, J. Yamasaki, T. Mizugaki, T. Mitsudome, *Green Chem.* **2021**, *23*, 2010–2016.
[16] S. Yamaguchi, T. Mizugaki, T. Mitsudome, *Eur. J. Inorg. Chem.* **2021**, *2021*, 3327–3331.
[17] a) T. Soták, T. Schmidt, M. Hronec, *Appl. Catal. A* **2013**, *459*, 26–33; b) J. Sun, H. Liu, *Green Chem.* **2011**, *13*, 135–142; c) L. Zhao, J. H. Zhou, Z. J. Sui, X. G. Zhou, *Chem. Eng. Sci.* **2010**, *65*, 30–35.
[18] a) S. Cheng, S. I. Martínez-Monteagudo, *Asia-Pacific J Chem Eng* **2019**, *14*, e2275; b) G. F. Froment, J. de Wilde, K. B. Bischoff, *Chemical reactor analysis and design*, 3rd ed. ed., Wiley, Hoboken N. J., **2011**, 42-102.
[19] I. Bonnin, R. Méreau, T. Tassaing, F. Jérôme, K. de Oliveira Vigier, *ACS Sustainable Chem. Eng.* **2021**, *9*, 9240–9247.
[20] D. K. Mishra, A. A. Dabbawala, J. J. Park, S. H. Jhung, J.-S. Hwang, *Catal. Today* **2014**, *232*, 99–107.
[21] V. N. Sapunov, M. Y. Grigoryev, E. M. Sulman, M. B. Konyaeva, V. G. Matveeva, *The journal of physical chemistry. A* **2013**, *117*, 4073–4083.
[22] R. Palkovits, K. Tajvidi, J. Procelewska, R. Rinaldi, A. Ruppert, *Green Chem.* **2010**, *12*, 972.
[23] L.-N. Ding, A.-Q. Wang, M.-Y. Zheng, T. Zhang, *ChemSusChem* **2010**, *3*, 818–821.
[24] M. Qiu, J. Zheng, Y. Yao, L. Liu, X. Zhou, H. Jiao, J. Aarons, K. Zhang, Q. Guan, W. Li, *J. Cleaner Prod.* **2022**, *362*, 132364.
[25] a) F. Geng, Y. Bonita, V. Jain, M. Magiera, N. Rai, J. C. Hicks, *Ind. Eng. Chem. Res.* **2020**, *59*, 6931–6943; b) S. Sawhill, *J. Catal.* **2003**, *215*, 208–219.
[26] Q. Qian, W. Wang, G. Wang, X. He, Y. Feng, Z. Li, Y. Zhu, Y. Zhang, G. Zhang, *Small (Weinheim an der Bergstrasse, Germany)* **2022**, *18*, e2200242.
[27] T. Suoranta, M. Niemelä, P. Perämäki, *Talanta* **2014**, *119*, 425–429.
[28] J. Schindelin et al., *Nat. Methods* **2012**, *9*, 676–682.
[29] a) C. Hernandez-Mejia, E. S. Gnanakumar, A. Olivos-Suarez, J. Gascon, H. F. Greer, W. Zhou, G. Rothenberg, N. Raveendran Shiju, *Catal. Sci. Technol.* **2016**, *6*, 577–582; b) D. K. Mishra, A. A. Dabbawala, J.-S. Hwang, *Catal. Commun.* **2013**, *41*, 52–55; c) D. K. Mishra, A. A. Dabbawala, J.-S.

Research Article
doi.org/10.1002/ejic.202400117

Hwang, *J. Mol. Catal. A* **2013**, *376*, 63–70; d) V. A. Sifontes Herrera, O. Oladele, K. Kordás, K. Eränen, J.-P. Mikkola, D. Y. Murzin, T. Salmi, *J. Chem. Technol. Biotechnol.* **2011**, *86*, 658–668.
[30] B. Hunger, J. Hoffmann, O. Heitzsch, M. Hunger, *J. Therm. Anal.* **1990**, *36*, 1379–1391.
[31] Y. Román-Leshkov, M. E. Davis, *ACS Catal.* **2011**, *1*, 1566–1580.
[32] N. Katada, T. Tsubaki, M. Niwa, *Appl. Catal. A* **2008**, *340*, 76–86.
[33] a) Z.-J. Diao, L.-Q. Huang, B. Chen, T. Gao, Z.-Z. Cao, X.-D. Ren, S.-J. Zhao, S. Li, *Fuel* **2022**, *324*, 124489; b) Y. I. Galindo-Ortega, A. Infantes-Molina, R. Huirache-Acuña, I. Barroso-Martín, E. Rodríguez-Castellón, S. Fuentes, G. Alonso-Nuñez, T. A. Zepeda, *Fuel Process. Technol.* **2020**, *208*, 106507.
[34] G. Ertl, *Handbook of heterogeneous catalysis. 3.1.2 Particle Size and Dispersion Measurements*, 2., completely rev. and enl. ed. ed., WILEY-VCH, Weinheim, **2008**, 738–765.
[35] M. C. M. Castoldi, L. D. T. Câmara, D. A. G. Aranda, *React. Kinet. Catal. Lett.* **2009**, *98*, 83–89.
[36] S. Carlier, J. Gripekoven, M. Philippo, S. Hermans, *Appl. Catal. B* **2021**, *282*, 119515.
[37] C. Luo, S. Wang, H. Liu, *Angew. Chem. Int. Ed.* **2007**, *46*, 7636–7639.

Manuscript received: April 12, 2024
Accepted manuscript online: April 26, 2024
Version of record online: June 14, 2024